CELL BIOLOGY

Initial spindle positioning at the oocyte center protects against incorrect kinetochore-microtubule attachment and aneuploidy in mice

Jessica N. Kincade[1], Avery Hlavacek[1], Takashi Akera[2], Ahmed Z. Balboula[1]*

Spindle positioning within the oocyte must be tightly regulated. In mice, the spindle is predominantly assembled at the oocyte center before its migration toward the cortex to achieve the highly asymmetric division, a characteristic of female meiosis. The significance of the initial central positioning of the spindle is largely unknown. We show that initial spindle positioning at the oocyte center is an insurance mechanism to avoid the premature exposure of the spindle to cortical CDC42 signaling, which perturbs proper kinetochore-microtubule attachments, leading to the formation of aneuploid gametes. These findings contribute to understanding why female gametes are notoriously associated with high rates of aneuploidy, the leading genetic cause of miscarriage and congenital abnormalities.

INTRODUCTION

Infertility is a globally prevalent issue affecting approximately 122 million women worldwide (*1*). Errors in chromosome segregation during meiosis result in aneuploidy, the leading genetic cause of miscarriage and congenital birth defects such as Down syndrome (*2*, *3*). Given that chromosome segregation errors occur mostly in female meiosis, particularly during the first meiotic division [meiosis I (MI)] (*2*, *3*), it is crucial to understand the molecular mechanisms regulating female MI and how it can go wrong.

Oogenesis is a complex process that begins during fetal development in female mammalian species, shortly after conception. During late pregnancy, fetal oocytes enter MI and duplicate their genome DNA (*4*). Shortly after birth, all germ cells undergo a prolonged arrest at the prophase I stage, which lasts until puberty. In adult ovaries, hormonal cues before ovulation stimulate the oocyte to resume meiosis (*4*). In mice, rats, dogs, domestic cats, and blue fox, the nucleus (germinal vesicle, GV) typically localizes at the oocyte center in fully grown prophase I–arrested oocytes (*5*–*10*). In contrast, the majority of human, bovine, and porcine oocytes have a peripheral nucleus (*10*–*13*). Peripheral nucleus localization in both human and mouse oocytes correlates with reduced maturation rates (*10*). In mouse oocytes, if the nucleus is located off-center, these cortical nuclei can migrate toward the oocyte center by F-actin–mediated pressure gradient (*14*–*17*). Recent studies demonstrated that Formin 2 knockout oocytes (which lack F-actin and have off-centered nucleus positioning) showed altered global transcriptional dynamics, suggesting a role of nucleus centering in both the amount and the splicing of maternal transcripts (*17*, *18*). However, the significance of central nucleus positioning remains largely unknown.

Upon meiotic resumption, prophase I–arrested oocytes undergo nuclear envelope breakdown (NEBD). Because the spindle forms where NEBD occurs, the nucleus position substantially influences the location of the initial spindle assembly. Therefore, in mice, the spindle is mainly formed at the oocyte center. In contrast to somatic cells, mouse oocytes lack classic centrosomes and rely on acentriolar microtubule-organizing centers (MTOCs) to regulate bipolar spindle formation. Mouse oocytes contain three different classes of MTOCs. Both perinuclear MTOCs (class I) and a subset of cytoplasmic MTOCs (class II) contribute to bipolar spindle formation (*19*–*22*), whereas metaphase cytoplasmic MTOCs (mcMTOCs, class III) remain in the cytoplasm and play an important role in regulating spindle positioning (*23*). Because the spindle position dictates the cell division plane (*24*), the centrally located spindle must migrate to the oocyte cortex to ensure the extrusion of half of the chromosomes into a small polar body (PB) (*24*–*28*). This highly asymmetric cell division is critical, as it allows the oocyte to retain the majority of the cytoplasmic storage of maternal RNAs and proteins, which are essential for early embryonic development (*29*). However, it is still mysterious why the spindle initially forms at the oocyte center, especially because it can increase the risk of symmetric division, leading to infertility.

Here, we show that premature peripheral spindle positioning causes abnormal kinetochore-microtubule (K-MT) attachments, chromosome misalignment, aneuploidy, and impaired early embryonic development. We find that the initial spindle positioning at the oocyte center is critical to avoid the premature exposure of the spindle to cortical CDC42 signaling, which perturbs the fidelity of K-MT attachments through increased MT tyrosination.

RESULTS

Peripheral GV oocytes have higher rates of chromosome misalignment and aneuploidy in metaphase II oocytes

In mouse oocytes, the meiotic spindle can initially form at the oocyte center (fig. S1A) or near the cortex (fig. S1B), depending on where NEBD occurs. To investigate the impact of the initial spindle position on female meiosis, we sorted fully grown prophase I–arrested oocytes into three groups based on the shortest distance between the nucleus and the cortex: central (larger than 15 μm), intermediate (5 to 15 μm), and peripheral (less than 5 μm) GV oocytes (Fig. 1, A and B). Careful rolling of the oocyte, as previously

[1]Animal Sciences Research Center, University of Missouri, Columbia, MO 65211, USA. [2]Cell and Developmental Biology Center, National Heart, Lung, and Blood Institute, National Institutes of Health, Bethesda, MD 20892, USA.
*Corresponding author. Email: abalboula@missouri.edu

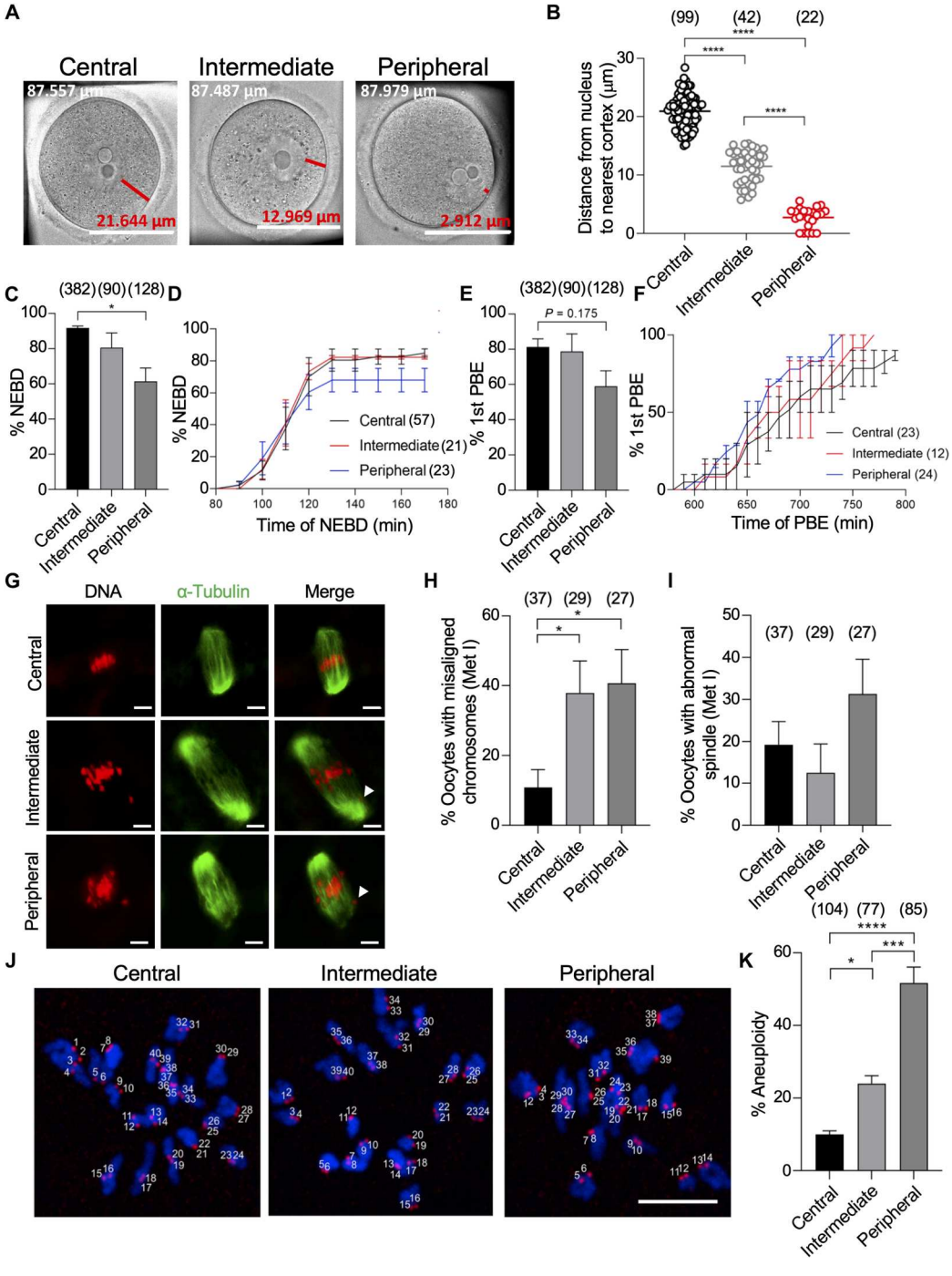

Fig. 1. Oocytes with a peripherally located nucleus have higher rates of chromosome misalignment and aneuploidy. (**A**) Full-grown germinal vesicle (GV) oocytes were sorted into central, intermediate, or peripheral GV oocytes. Scale bars, 50 µm. Oocyte diameter is included in the top left of each image (white text); distance from the nucleus to the cortex is included above the scale bar (red text). (**B**) Quantification of the average distance from the nucleus to the nearest cortex within groups. (**C** to **F**) Central, intermediate, and peripheral GV oocytes were imaged live using time-lapse microscopy during in vitro maturation (IVM) and assessed for the percentage of oocytes that underwent nuclear envelope breakdown (NEBD) (C), the average time of NEBD (D), the percentage of first polar body extrusion (1st PBE) (E), and the average time of PBE calculated from oocytes successfully extruded the PB (F). (**G** to **K**) Central, intermediate, and peripheral GV oocytes were in vitro matured for 7 hours (metaphase I) or 14 hours (metaphase II). Metaphase I oocytes were immunostained with α-tubulin to label the spindle. Metaphase II oocytes were assessed for aneuploidy. Oocytes containing greater or less than 40 kinetochores (stained with CREST) were scored as aneuploid. DNA was labeled by 4′,6-diamidino-2-phenylindole (DAPI). (G) Representative confocal images of metaphase I oocytes. (H) Quantification of the percentage of chromosome misalignment in (G). (I) Quantification of the percentage of abnormal spindle morphology in (G). (J) Representative images of metaphase II oocytes assessed for aneuploidy. (K) Quantification of the percentage of aneuploidy. Scale bar, 10 µm. One-way analysis of variance (ANOVA) and Tukey's post hoc tests were performed to determine statistical significance among groups. Data are displayed as means ± SEM. Values with asterisks vary significantly, $*P < 0.05$; $***P < 0.001$; $****P < 0.0001$. The total number of analyzed oocytes (from at least three independent replicates) is specified in each graph.

described (*5*), ensured the correct classification. All oocytes selected for the following experiments were comparable in size with a diameter larger than 80 µm (fig. S1, C and D), indicating the full-grown status (*30*). Any oocyte with a diameter less than 80 µm was removed from further experiments to exclude the possibility of oocyte growth-associated nucleus centration (*5*). DNA staining revealed that all selected oocytes, including peripheral GV oocytes, had a surrounded nucleolus (fig. S1E), a criterion positively associated with developmental competence (*31*). Last, central GV oocytes were more common compared to intermediate GV oocytes and peripheral GV oocytes (fig. S1F).

Using the sorted oocytes, we examined the impact of the nucleus position on female meiosis. To examine meiotic progression, oocytes were collected from mice aged 6 to 8 weeks and matured for 16 hours (metaphase II). The majority (~92%) of central GV oocytes were able to undergo NEBD. In contrast, peripheral GV

oocytes showed a significant decrease in the NEBD rate (~61%; Fig. 1C). However, using time-lapse microscopy, we found no significant difference in the timing of NEBD between central GV oocytes and peripheral GV oocytes (Fig. 1D). Similarly, a majority (~81%) of central GV oocytes were able to extrude the first PB (PBE), while peripheral GV oocytes were less successful in extruding the first PB (~60%; Fig. 1E). Once again, there was no significant difference in the timing of PBE between central GV oocytes and peripheral GV oocytes (Fig. 1F). To examine the chromosome alignment and spindle morphology among these groups, oocytes were matured in vitro for either 7 (metaphase I) or 16 hours (metaphase II). Chromosome alignment was examined on the basis of the parameters previously described (*32*). We found a significant increase in chromosome misalignment at both metaphase I and metaphase II in peripheral GV oocytes, compared to central GV oocytes (Fig. 1, G and H, and fig. S2, A and B). Intermediate GV oocytes also showed significantly higher rates of chromosome misalignment when compared to central GV oocytes at metaphase I but not at metaphase II (Fig. 1, G and H, and fig. S2, A and B). Spindle morphology did not vary significantly among these groups either at metaphase I or metaphase II (Fig. 1, G and I, and fig. S2, A and C). Because chromosome misalignment is highly associated with aneuploidy, we then assessed aneuploidy in metaphase II oocytes using in situ chromosome counting (*33*, *34*). Notably, segregation errors occurred in peripheral GV oocytes (~50%) approximately five times more frequently than in central GV oocytes (~8%; Fig. 1, J and K). Although we cannot exclude the impact of additional manipulating time (~30 min for oocyte sorting/measurements) on oocyte quality, ~8% aneuploidy in central GV oocytes remains within the range of aneuploidy in control groups in several previous publications (*35*, *36*). To further investigate the developmental competence of peripheral GV oocytes, we parthenogenetically activated in vitro matured central and peripheral oocytes, followed by assessing the subsequent embryo development. We found that the cleavage rate (two- and four-cell parthenotes) of parthenogenetically activated peripheral GV oocytes was significantly lower (~60%) than that of central GV oocytes (~87%; fig. S2D), indicating that the developmental competence is compromised in peripheral GV oocytes.

Incorrect K-MT attachments are increased in oocytes with a peripherally located nucleus

One important cause of aneuploidy is the weakened spindle assembly checkpoint (SAC). Typically, the SAC monitors the status of K-MT attachments and will become inactivated when MTs are correctly attached to all kinetochores. However, a weakened SAC may allow the progression of the cell to anaphase before proper K-MT attachments are established, leading to aneuploidy. To assess the SAC function in central, intermediate, and peripheral GV oocytes, oocytes were treated with nocodazole, an MT-depolymerizing drug that maintains the SAC active and thereby impairs PBE by inducing metaphase I arrest (*34*, *37*). We found that the majority of central, intermediate, and peripheral GV oocytes failed to extrude the PB in the presence of a low dose of nocodazole (400 nM) (*38*). In contrast, in the positive control groups where unsorted or peripheral GV oocytes were treated with ZM447439, an Aurora kinase B/C inhibitor that is known to disrupt the SAC function at a high dose (10 μM) (*38*), the PB was extruded in the majority of unsorted or peripheral GV oocytes even in the presence of nocodazole (fig. S2E). These results suggest that the SAC is intact in peripheral GV oocytes, and therefore does not explain their observed high aneuploidy rate.

Following spindle migration to the cortex along its longitudinal axis, centromeres facing the cortex have less stable K-MT attachments (*39*). These observations suggest that the cortex can influence MT dynamics and their ability to establish stable attachments with kinetochores (*39*), a critical step to ensure faithful chromosome segregation. In oocytes, even if the SAC is satisfied by present K-MT attachments, it is not necessary that all attachments are correct and homologous chromosomes are bioriented (*32*). To assess K-MT attachments, metaphase I oocytes were exposed to a brief cold shock (6 min) to depolymerize labile non–K-MTs and preferentially maintain stable MT fibers that are attached to kinetochores (K-fibers) (*34*). Nucleus positioning had no effect on the percentage of unattached kinetochores (Fig. 2A and fig. S2F). However, peripheral GV oocytes displayed an approximately fourfold increase in the percentage of incorrect K-MT attachments, compared to central GV oocytes (Fig. 2, A and B). Moreover, the percentages of peripheral (37.93 ± 9.17%) and intermediate (39.13 ± 10.41%) GV oocytes having two or more abnormally attached kinetochores were significantly higher than those in central GV oocytes (7.14 ± 4.02%; Fig. 2C). To examine K-fiber stability in peripheral GV oocytes, we assessed the resistance of K-fibers to disassembly after a relatively longer exposure to cold shock (10 min). Peripheral GV oocytes showed significantly reduced K-fiber stability when compared to central GV oocytes (fig. S2, G to I). These results suggest that improper K-MT attachments due to the less stable K-fibers are the likely cause, at least in part, of decreased PBE and increased aneuploidy rates in peripheral GV oocytes.

Prophase I oocytes favor central nucleus positioning

When meiotic resumption was prevented (by milrinone treatment) in peripheral GV oocytes, the nucleus relocated to the oocyte center within 3 hours of incubation in the majority of oocytes (fig. S3, A and B, and movie S1), confirming that the nucleus favors the central position, as previously reported (*14*, *40*). Central positioning of the nucleus is actin dependent. However, there were no differences observed between oocytes with a centrally or a peripherally located nucleus in terms of cytoplasmic F-actin, cortical F-actin, or perinuclear F-actin (fig. S3, C to F). When the oocytes were allowed to resume meiosis, in milrinone-free medium, nuclei initially located at the periphery of the oocyte underwent significant central movement (10 ± 1.256 μm) before NEBD. Intermediately located nucleus and centrally located nucleus also underwent centration and traveled a distance of 6 ± 0.6024 and 4 ± 0.6783 μm, respectively, before NEBD (fig. S4A). However, even with the significant central movement, the chromosomes remained relatively closer to the cortex at the time of alignment in peripheral GV oocytes, compared to central GV oocytes (fig. S4, B and C, and movies S2 and S3). It is of note that the timing of chromosome alignment did not vary significantly among groups (fig. S4D). These results suggest that mouse oocytes favor central nucleus positioning, likely to avoid the increased incidence of aneuploidy in peripheral GV oocytes.

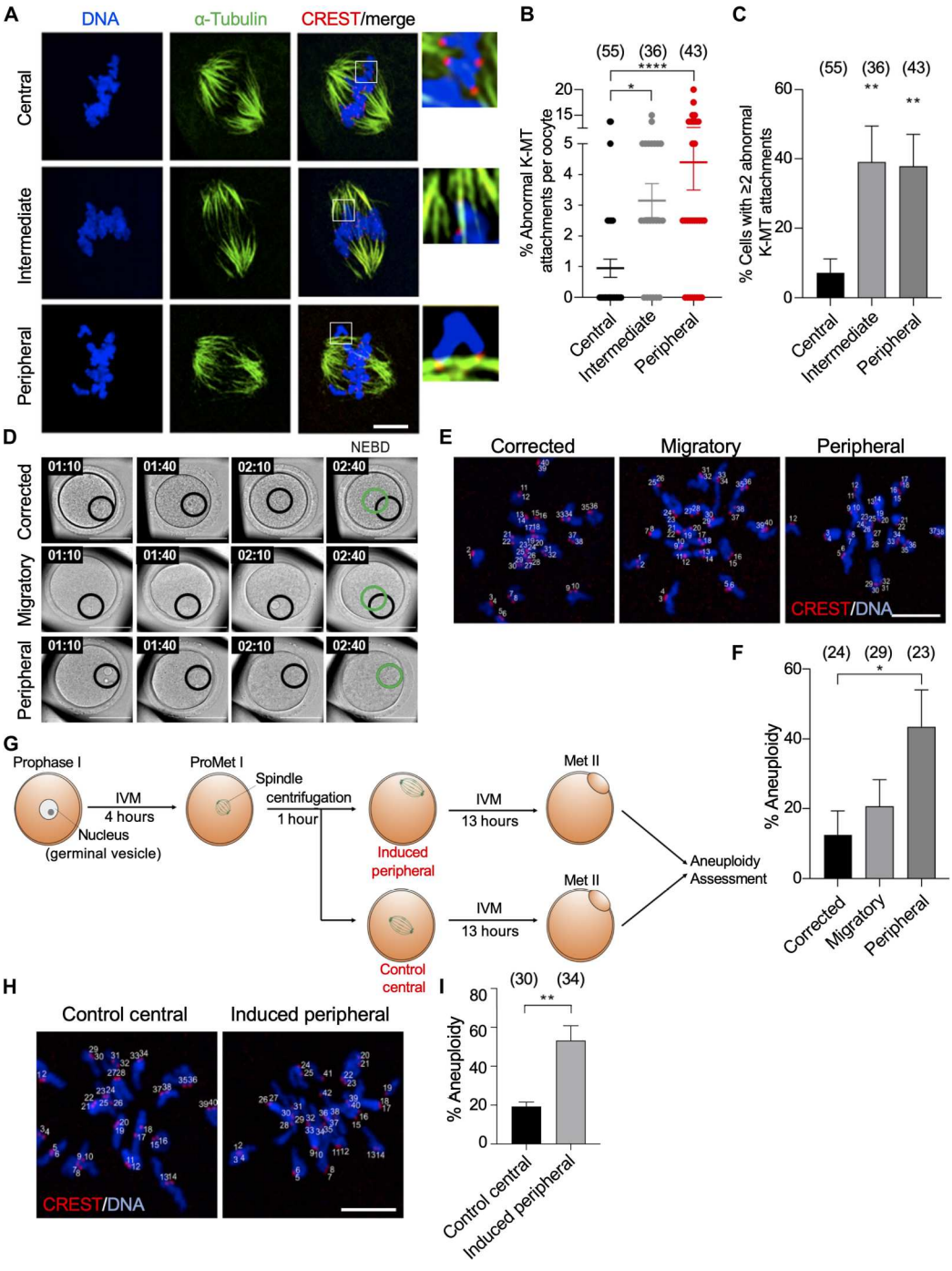

Fig. 2. Incidence of incorrect K-MT attachments and aneuploidy associate with spindle proximity to the cortex. (**A**) Representative confocal images of kinetochore-microtubule (K-MT) attachments in central, intermediate, or peripheral GV oocytes matured to metaphase I and immunostained with α-tubulin (to label MTs) and CREST (to label kinetochores). DNA was stained with DAPI. Scale bar, 10 μm. (**B**) Quantification of abnormal K-MT attachments. (**C**) Quantification of the oocytes with two or more incorrect K-MT attachments. One-way ANOVA and Tukey's post hoc test were performed to analyze the data. (**D**) Representative images of the nucleus movement before NEBD. The black circle denotes the primary nucleus positioning, while the green circle denotes the final nucleus position before NEBD. Scale bars, 50 μm. (**E**) Representative images of aneuploidy in oocytes experiencing full migration of the nucleus (corrected/central), attempted migration of their nucleus (migratory), or not attempting central migration of the nucleus (peripheral). Scale bar, 10 μm. (**F**) Quantification of the incidence of aneuploidy in metaphase II oocytes from the oocytes categorized in (D). One-way ANOVA and Tukey's post hoc test were performed to analyze the data. (**G**) Schematic depicting the induction of peripheral spindle positioning by mild centrifugation of central GV oocytes. (**H**) Representative images of aneuploidy in oocytes either maintaining central spindle positioning after centrifugation or induced peripheral spindle positioning after centrifugation. Scale bar, 10 μm. (**I**) Quantification of the incidence of aneuploidy in oocytes with induced peripherally positioned nucleus and centrally positioned nucleus after centrifugation. Student's *t* test was performed to determine statistical significance. Data are displayed as means ± SEM. Values with asterisks vary significantly, $^{*}P < 0.05$; $^{**}P < 0.01$; $^{****}P < 0.0001$. The total number of analyzed oocytes (from at least three independent replicates) is specified above each graph.

Incidence of aneuploidy correlates with the proximity of early spindle positioning to the cortex

Because the spindle forms where NEBD occurs, whether at the center (fig. S1A) or at the cortex (fig. S1B), it is likely that increased aneuploidy in peripheral GV oocytes is, at least in part, due to peripheral spindle formation. Using live time-lapse microscopy, we found that oocytes with a peripherally located nucleus demonstrate one of three types of movement: Oocytes that were able to achieve complete relocation of the nucleus to the center before NEBD (the spindle is formed centrally) were termed "corrected," oocytes that demonstrated central movement before NEBD but did not achieve full relocation were termed "migratory," and oocytes that failed to make a relocation attempt before NEBD and remained at the cortex were termed "peripheral" (the spindle is formed peripherally; Fig. 2D). Notably, although all oocytes selected in this experiment were peripheral GV oocytes, oocytes that were able to

successfully relocate their nucleus to the center and experienced central spindle formation showed relatively lower rates of aneuploidy when compared to oocytes that failed nucleus relocation and underwent NEBD at the periphery of the oocyte (Fig. 2, E and F). These results suggest that peripheral GV oocytes are not inherently erroneous, but instead peripheral spindle formation is detrimental to the fidelity of chromosome segregation.

After meiotic resumption, mouse oocyte spindles are typically formed and remained at the oocyte center until late metaphase I, followed by their timely migration toward the cortex. It is technically feasible to shift the position of the spindle within the oocyte without noticeable adverse effects (*28*). To further confirm the relationship between the aneuploidy rate and the proximity of early spindle positioning to the cortex, we experimentally relocated the spindle prematurely to the cortex through mild centrifugation (Fig. 2G). This centrifugation technique has been used extensively for several purposes (e.g., lipid droplet removal and before parthenogenetic activation) without noticeable detrimental effects on oocyte developmental competence (*41*–*43*). Central GV oocytes were selected and matured in vitro for 4 hours, until prometaphase I (the time before establishing correct K-MT attachments) (*44*). These prometaphase I oocytes were centrifuged, examined live under the microscope, and resorted into two groups according to their spindle positioning: those maintaining central positioning (control central) and those with induced peripheral positioning (induced peripheral), which was followed by further in vitro maturation (IVM) to reach metaphase II. Although all oocytes were originally central GV oocytes, oocytes with induced peripheral positioning showed significantly higher rates of aneuploidy when compared to oocytes maintaining central spindle positioning after centrifugation (Fig. 2, H and I), indicating that the premature cortical proximity of the spindle (before establishing correct K-MT attachments) causes erroneous chromosome segregation.

Premature exposure to the cortical CDC42 signaling perturbs K-MT attachments in oocytes

The increased incidence of chromosome missegregation when the spindle is formed near the cortex suggests the involvement of cortical signaling in perturbing K-MT attachments. The proximity of chromosomes to the oocyte cortex, after spindle migration, induces Ras-related Nuclear Protein–guanosine triphosphate (RAN-GTP)–dependent cortical enrichment of several factors such as active CDC42 and RAC guanosine triphosphatases (CDC42-GTP and RAC-GTP), which subsequently contribute to establishing oocyte polarity (*45*, *46*). Typically, RAC-GTP and CDC42-GTP are enriched at the oocyte cortex only after chromosomes reach the cortex upon spindle migration (at late metaphase I). We first examined whether CDC42 and/or RAC are precociously activated locally at the oocyte cortex in peripheral GV oocytes. Central and peripheral GV oocytes were matured in vitro for 5 hours (3 hours after NEBD, prometaphase I), and oocytes with a centrally and peripherally positioned spindle (confirmed using Z-series live imaging) were sorted and examined for active CDC42 and RAC. To assess RAC-GTP, the oocytes were microinjected with RAC biosensor [P21-Activated Kinase–yellow fluorescent protein (PAK-YFP)], a specific probe to assess RAC-GTP in mouse oocytes (*45*), whereas Neural Wiskott-Aldrich Syndrome Protein (N-WASP), a recognized GTP-CDC42 binding protein, was used as a readout of CDC42-GTP (*46*). Both PAK-YFP (fig. S5, A to C) and N-WASP (Fig. 3, B to D) were precociously enriched at the cortex of prometaphase I oocytes with a peripherally located spindle but not at the cortex of those with a centrally located spindle. To investigate whether the premature exposure of the spindle to cortical CDC42 and/or RAC signaling perturbs the establishment of correct K-MT attachments, we inhibited CDC42 or RAC signaling in prometaphase I oocytes (the stage at which the majority of abnormal K-MT attachments are corrected) with a peripherally located spindle. Peripheral GV oocytes were matured in vitro for 5 hours, and oocytes with a peripherally positioned spindle (confirmed using Z-series live imaging) were selected and treated (for an additional 2 hours) with ML141 (Fig. 3A), a previously proven selective CDC42 inhibitor in mammalian oocytes (*47*–*50*). Treating peripheral GV oocytes with ML141 efficiently abolished N-WASP enrichment at the oocyte cortex (Fig. 3, B to D). Examining K-MT attachments in metaphase I oocytes showed that CDC42 inhibition did not affect the number of unattached kinetochores among groups (fig. S5D) or K-MT attachments in oocytes with a centrally located spindle (Fig. 3, E and F). Inhibition of cortical CDC42 signals using ML141 significantly rescued abnormal K-MT attachments (Fig. 3, E and F) and reduced K-fiber stability (fig. S2, G to I) in oocytes with a peripherally positioned spindle, without affecting cytoplasmic or cortical F-actin in those peripheral oocytes (fig. S6, A to C). To confirm this finding, we perturbed the CDC42 signaling by overexpressing a CDC42 dominant-negative mutant (CDC42 T17N; previously demonstrated to inhibit GTP-CDC42 in mouse oocytes) (*46*). Consistent with the ML141 results, perturbing CDC42 signaling by overexpressing CDC42 dominant-negative mutant significantly rescued abnormal K-MT attachments in oocytes with a peripherally located spindle (Fig. 3, G and H). To further confirm the impact of CDC42 signaling on K-MT attachments, we examined whether expressing constitutively active CDC42 (which was previously shown to ectopically enrich its downstream target, N-WASP, at the entire oocyte cortex and in cytoplasmic vesicles) (*46*) perturbs K-MT attachments in oocytes with a centrally located spindle. Expressing constitutively active CDC42 mutant (CDC42 Q61L) significantly increased abnormal K-MT attachments in oocytes with a centrally located spindle (Fig. 3, I and J), further confirming the involvement of CDC42 signaling in perturbing the establishment of correct K-MT attachments. On the other hand, inhibiting RAC signaling in oocytes with a peripherally located spindle by expressing a RAC dominant-negative mutant (RAC T17N; previously demonstrated to inhibit RAC-GTP in mouse oocytes) (*45*) did not rescue the increased incidence of abnormal K-MT attachments in oocytes with a peripherally located spindle (fig. S5, E and F). Together, these results suggest that the increased incidence of abnormal K-MT attachments in oocytes with a peripherally located spindle is, at least in part, due to the premature exposure of the spindle to cortical CDC42 signaling.

Induced peripheral oocytes (i.e., oocytes with a peripherally located spindle after centrifugation) exhibited higher rates of abnormal K-MT attachments, compared to those that maintained a centrally positioned spindle (control central) after centrifugation (fig. S7, A and C). To confirm that K-MT attachments in induced peripheral oocytes were affected primarily by the proximity to the cortex and to exclude the possibility that the difference in the response to centrifugation between induced peripheral and control central oocytes was due to a preexisting difference, we determined whether inhibiting cortical CDC42 signaling could rescue the

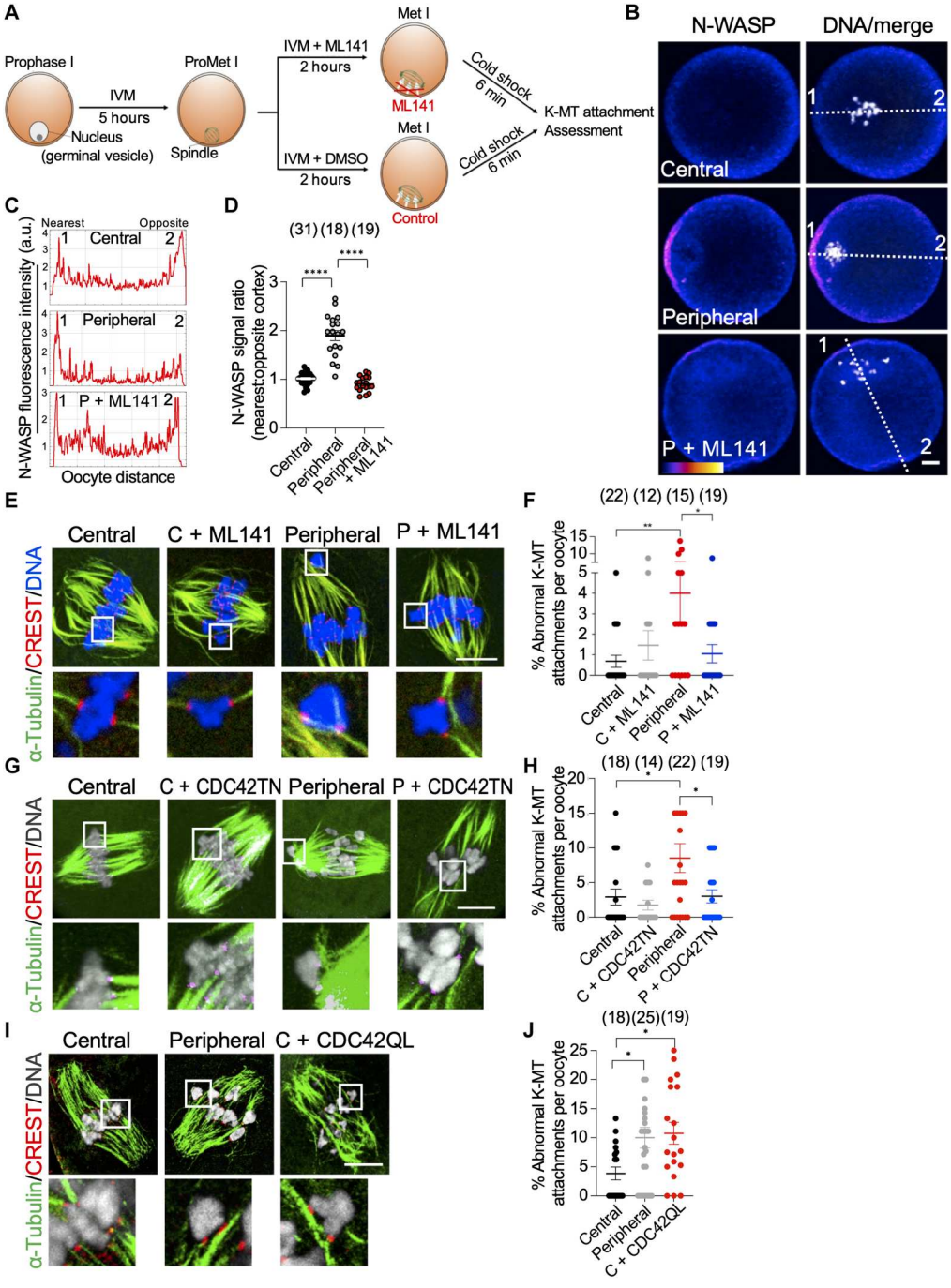

Fig. 3. Cortical CDC42 signaling impairs proper K-MT attachments in oocytes with peripherally located spindles. (**A**) Schematic depicting the treatment of oocytes with ML141, a CDC42 inhibitor, before assessing K-MT attachments. (**B**) Representative confocal (single-slice) images of prometaphase I central, peripheral, and ML141-treated peripheral oocytes (ML141 was added at NEBD). The oocytes were immunostained with N-WASP antibody. The DNA was stained with DAPI. (**C**) Examples of N-WASP fluorescence intensity in (B). a.u., arbitrary units. (**D**) N-WASP cortical enrichment was quantified as the ratio of N-WASP intensity at the cortical side closest to the chromosomes to N-WASP intensity at the cortical side opposite to chromosome localization. (**E**) Representative images of dimethyl sulfoxide (DMSO) and ML141-treated oocytes matured to metaphase I and assessed for K-MT attachments. (**F**) Quantification of abnormal K-MT attachments for the oocyte populations is illustrated in (E). (**G**) Representative images of K-MT attachments in central and peripheral oocytes as well as central and peripheral oocytes expressing CDC42T17N. Full-grown GV oocytes were collected and immediately microinjected with Cdc42T17N complementary RNA (cRNA) during IVM (in the absence of milrinone). Metaphase I oocytes were assessed for K-MT attachments. (**H**) Quantification of abnormal K-MT attachments for the oocyte populations is illustrated in (G). (**I**) Representative images of K-MT attachment in central, peripheral, and central oocytes expressing CDC42QL. Full-grown GV oocytes were collected and immediately microinjected with Cdc42Q61L cRNA during IVM. Metaphase I oocytes were assessed for K-MT attachments. (**J**) Quantification of abnormal K-MT attachments for the oocyte populations is illustrated in (I). Scale bars, 10 μm. One-way ANOVA and Tukey's post hoc test were performed to determine statistical significance. Data are displayed as means ± SEM. Values with asterisks vary significantly, $*P < 0.05$; $**P < 0.01$; $****P < 0.0001$. The total number of analyzed oocytes (from three independent replicates) is specified above each graph.

increased incidence of abnormal K-MT attachments in induced peripheral oocytes. Control central and induced peripheral prometaphase I (5 hours) oocytes were treated with or without ML141 for an additional 2 hours before assessing K-MT attachments (fig. S7A). There were no differences in the percentage of unattached kinetochores among groups (fig. S7B). CDC42 inhibition significantly rescued the increased incidence of abnormal K-MT attachments in induced peripheral oocytes (fig. S7C), further supporting the idea that increased abnormal K-MT attachments in induced peripheral oocytes is due to the premature exposure of the spindle to the cortical CDC42 signaling. Collectively, these results strongly suggest that avoiding the cortical CDC42 signaling during prometaphase I (i.e., by being at the oocyte center before timely spindle migration) is critical in protecting the oocyte's ability to establish correct K-MT attachments, leading to faithful chromosome segregation.

Excessive MT tyrosination interferes with establishing correct K-MT attachments

We next determined how cortical CDC42-GTP affects K-MT attachments. Because the cortical CDC42-GTP activates the Actin-Related Protein 2/3 (ARP2/3) complex, which plays an essential role in actin cap formation at the cortex (*46*, *51*), we tested whether CDC42 signaling perturbs K-MT attachments in peripheral GV oocytes via the premature activation of ARP2/3. To address this question, peripheral GV oocytes were matured in vitro for 5 hours, and oocytes with a peripherally positioned spindle (confirmed using Z-series live imaging) were treated with CK-666 (a selective and potent ARP2/3 inhibitor) (*51*) for an additional 2 hours. Analyzing K-MT attachments in metaphase I oocytes showed that ARP2/3 inhibition did not rescue abnormal K-MT attachments in oocytes with a peripherally located spindle (fig. S8, A and B), indicating that CDC42 signaling does not perturb the establishment of K-MT attachments via actin cap formation.

A recent study using mouse oocytes suggested that CDC42-GTP can promote α-tubulin tyrosination within the cortical spindle, increasing MT dynamics (*39*). Therefore, we hypothesized that the premature exposure of the spindle to cortical CDC42 signaling (i.e., before establishing correct K-MT attachments) results in excessive MT tyrosination, which interferes with the correction mechanism of K-MT attachments. The genetically encoded C-terminal tyrosine on α-tubulin undergoes cycles of detyrosination and (re)-tyrosination (*52*). In mitotic cells, initial incorrect attachments are established during prometaphase and primarily formed by tyrosinated MTs. Tyrosinated MTs are relatively labile to depolymerization, leading to their detachment from chromosomes. When correct attachments are established, MTs are detyrosinated and stabilized (*53*). In mouse oocytes, reducing α-tubulin tyrosination (by depleting tubulin-tyrosine ligase) increased the rate of MT stabilization (*39*). Thus, the level of MT tyrosination must be spatiotemporally regulated to establish correct K-MT attachments. Given the reduced K-fiber stability in oocytes with a peripherally located spindle (fig. S2, G to I), we determined whether α-tubulin tyrosination levels depend on the spindle position. In contrast to β-tubulin levels, which were not affected by the spindle position, tyrosinated α-tubulin levels were significantly higher in oocytes with a peripherally positioned spindle when compared to oocytes with a centrally positioned spindle (Fig. 4, A and B). We also confirmed the impact of CDC42 signaling on α-tubulin tyrosination in the spindle. Our results showed that tyrosinated α-tubulin levels were significantly lower in CDC42-inhibited oocytes (oocytes expressing CDC42 dominant-negative mutant, CDC42 T17N), compared to control oocytes (Fig. 4, C and D). Thus, CDC42-GTP promotes MT tyrosination in mouse oocytes. We then determined whether decreasing tyrosination levels could rescue increased abnormal K-MT attachments in peripheral GV oocytes. Removing the tyrosine residue from α-tubulin (i.e., detyrosination) is regulated by tubulin carboxypeptidase enzymes encoded by vasohibins (VASHs) (*54*, *55*). Ectopic expression of VASH2 did not completely abolish tyrosinated α-tubulin in mouse oocytes (Fig. 4E), whereas coexpression of VASH2 and small VASH binding protein (SVBP; a chaperone protein required for VASH stability) (*54*, *55*) eliminated tyrosinated α-tubulin (Fig. 4, E to G, and fig. S8C). Ectopic expression of VASH2/SVBP had no significant effect ($P = 0.75$) on the bipolar spindle formation (81.70 ± 1.7%, $n = 27$) when compared to control oocytes (84.35 ± 7.3%, $n = 25$). Decreasing α-tubulin tyrosination partially rescued abnormal K-MT attachments in oocytes with a peripherally located spindle (Fig. 4, H and I). Together, our data indicate that the premature exposure of the spindle to cortical CDC42 signaling interferes with the establishment of correct stable K-MT attachments, at least in part, via promoting MT tyrosination.

DISCUSSION

Aneuploidy occurs frequently in female meiosis, typically as a result of missegregation during MI (*2*, *3*, *56*). We developed different complementary and confirmatory oocyte models in which (i) the spindle is assembled peripherally or centrally (based on the nucleus position or the location of the spindle at NEBD), (ii) the centrally positioned spindle is prematurely relocated toward the cortex (using centrifugation), or (iii) the CDC42 signaling is perturbed in oocytes with a peripherally located spindle. We found that initial spindle positioning at the oocyte center (until proper K-MT attachments are established and before timely spindle migration) is an insurance mechanism to avoid the premature exposure to cortical CDC42 signaling, which induces excessive tubulin tyrosination and subsequently hinders proper K-MT attachments, leading to aneuploidy (Fig. 5). These findings may explain why, in mouse oocytes, correct K-MT attachments are primarily established when the spindle is still at the oocyte center (~2 hours before anaphase I), i.e., before migrating to the cortex (*39*, *44*).

In mouse oocytes, the spindle is mainly assembled at the oocyte center before migrating timely toward the oocyte cortex by F-actin–mediated mechanisms. Cytoplasmic F-actin is enriched around the spindle and chromosomes to drive their migration toward the cortex (*26*–*28*). We found that cytoplasmic F-actin is significantly lower in oocytes with a peripherally located spindle, compared to oocytes with a centrally located spindle (fig. S6, A to C). Therefore, it is tempting to speculate that this cytoplasmic F-actin enrichment does not occur in peripheral oocytes, because the spindle is already located near the cortex. The CDC42 inhibition reduced cytoplasmic F-actin in central oocytes, but not in peripheral oocytes, raising the possibility that the cytoplasmic F-actin enrichment is regulated, at least in part, by CDC42 signaling. Consistent with this hypothesis, CDC42 inhibition prevents spindle migration toward the cortex in mouse oocytes (*57*). It would be an interesting future direction to study how the spindle position can affect the enrichment of cytoplasmic F-actin. Another interesting future direction is to investigate how CDC42-GTP promotes MT tyrosination. We speculate two possible models: (i) CDC42-GTP increases the activity of tubulin tyrosine ligase, which catalyzes tyrosination (*58*, *59*), specifically near the cortex or (ii) CDC42-GTP locally inhibits the activity of the detyrosination enzyme, VASH/SVBP, to relatively increase tyrosination near the cortex (*54*, *55*). Understanding the molecular mechanisms underlying how the CDC42 signaling regulates cytoplasmic F-actin and MT tyrosination would lead to a deeper understanding of how oocyte meiosis is regulated and how it can go wrong.

Nucleus relocation within eukaryotic cells is critical for organism development. In *Drosophila* oocytes, the nucleus migrates from a central posterior to an asymmetrical anterior position to dictate the dorsal-ventral axis, which is necessary for subsequent embryo development (*60*). In *Caenorhabditis elegans* zygotes, the two pronuclei meet at the posterior cortex and then migrate

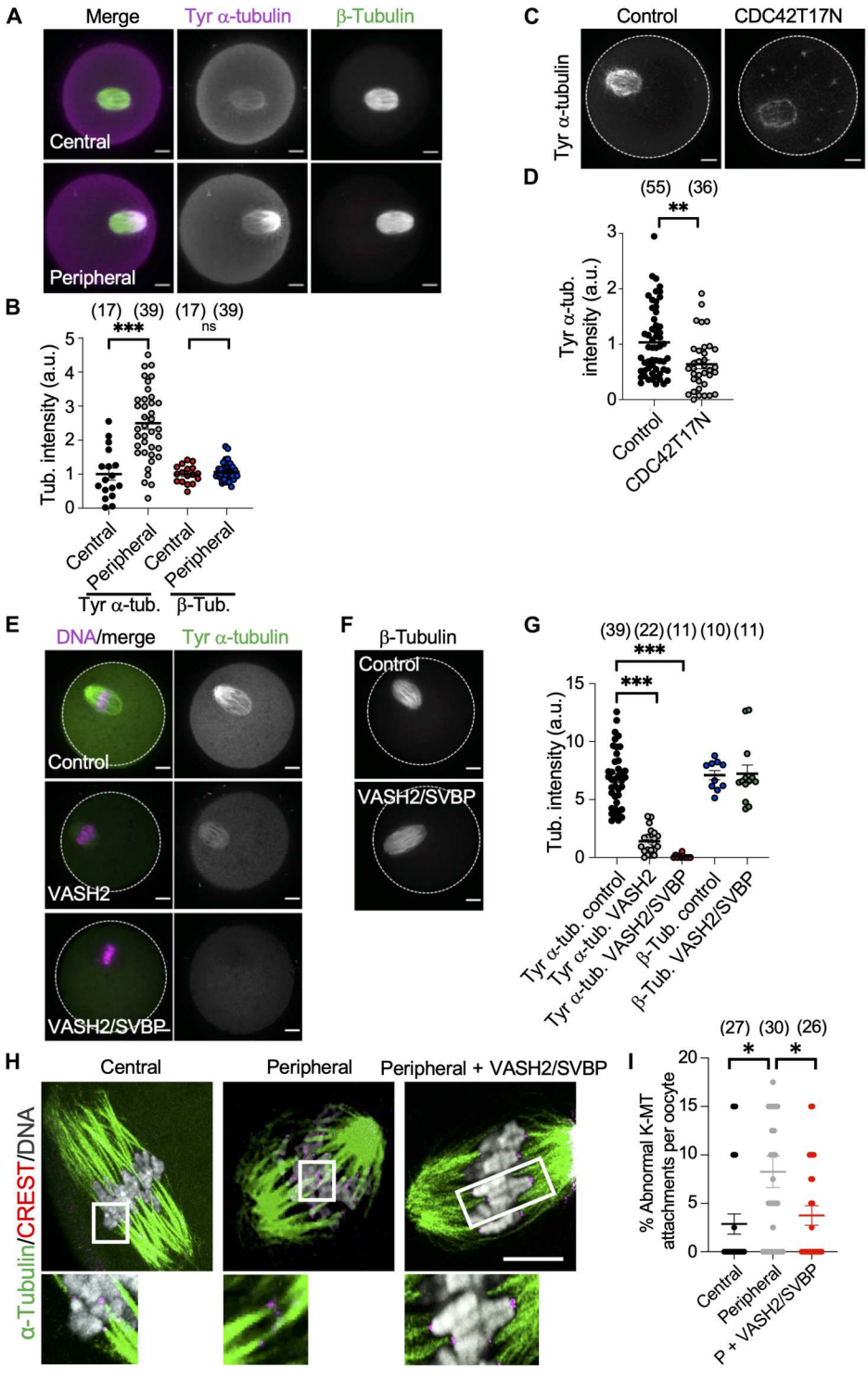

Fig. 4. Reducing tubulin tyrosination in peripheral GV oocytes rescued the abnormal K-MT attachments. (**A**) Representative images of oocytes with centrally and peripherally located spindles stained for tyrosinated α-tubulin and β-tubulin. (**B**) Quantification of tubulin intensities within the spindle. n.s., not significant. (**C**) Representative images of a control oocyte and an oocyte expressing CDC42 dominant-negative mutant (CDC42T17N) stained for tyrosinated α-tubulin. (**D**) Quantification of tyrosinated α-tubulin levels within the spindle for the oocyte populations is illustrated in (C). (**E** to **G**) Full-grown GV oocytes were microinjected with vasohibin 2 (VASH2)/small VASH binding protein (SVBP) cRNAs and cultured overnight in the presence of milrinone to prevent meiotic resumption before allowing the oocytes to mature (in the absence of milrinone) to metaphase I stage. Representative images of oocytes expressing VASH2 and VASH2/SVBP stained for tyrosinated α-tubulin (E) and β-tubulin (F). (G) Quantification of tubulin intensities within the spindle for the oocyte populations is illustrated in (E) and (F). (**H**) Representative images of K-MT attachments in a central GV oocyte (as a control), a peripheral GV oocyte, and a peripheral GV oocyte expressing VASH2 and VASH2/SVBP. Full-grown GV oocytes were collected and immediately microinjected with VASH2/SVBP cRNAs during IVM (in the absence of milrinone). Metaphase I oocytes were fixed and assessed for K-MT attachments. (**I**) Quantification of abnormal K-MT attachments for the oocyte populations is illustrated in (H). Scale bars, 10 μm. One-way ANOVA and Tukey's post hoc test were performed to determine statistical significance. Data are displayed as means ± SEM. Values with asterisks vary significantly, $^{*}P < 0.05$; $^{**}P < 0.01$; $^{***}P < 0.001$. The total number of analyzed oocytes is specified above each graph.

toward the zygote center to allow proper spindle pole orientation along the anterior-posterior axis before spindle migration toward the posterior cortex (*61*, *62*). Although mammalian oocytes at prophase I are not polarized and the nucleus position has no consequence on the developmental axis, mouse oocytes, the only studied mammalian system, still use nucleus relocation, which correlates with their maturation success (*5*, *10*). Following NEBD, the centrally formed spindle in mouse oocytes must migrate toward the cortex in a timely manner to ensure the asymmetric division. Our understanding of the biological significance of the initial central nucleus positioning is still rudimentary. It has been proposed that nucleus centration plays a role in keeping prophase I mouse oocytes in a nonpolarized state, ensuring random cytoplasmic distribution and avoiding unphysiological cytoplasmic compartmentalization

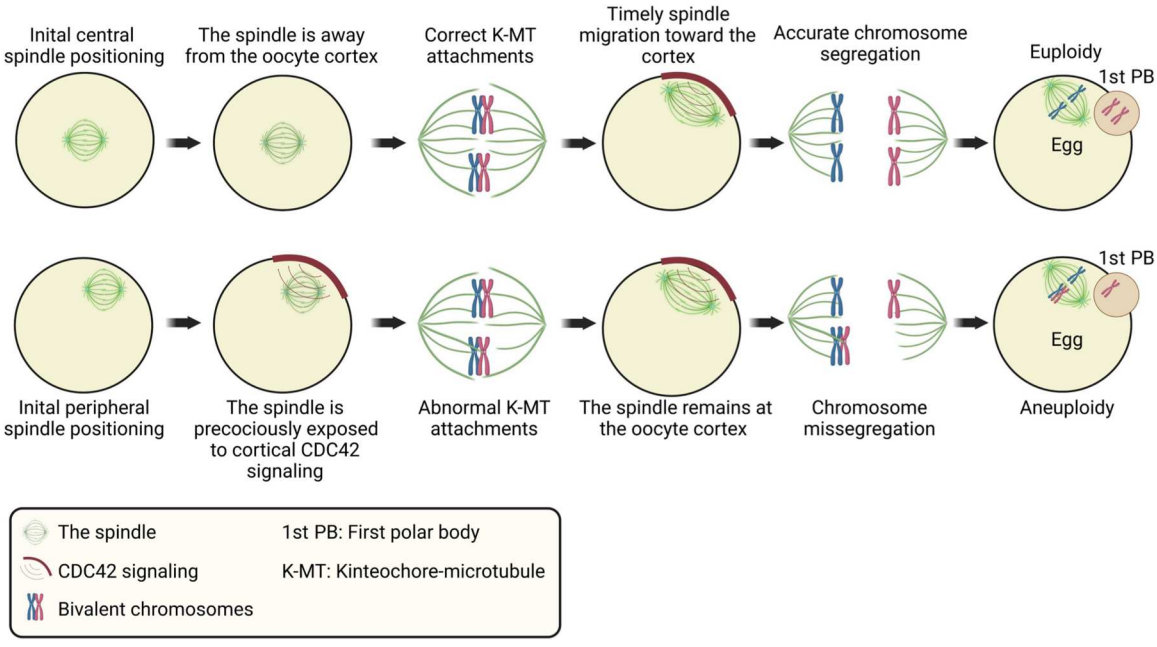

Fig. 5. Schematic model for the influence of initial spindle positioning on the fidelity of establishing correct K-MT attachments and aneuploidy incidence in mouse oocytes.

(*15*). Our findings suggest that central nucleus positioning is an insurance mechanism to avoid the premature exposure of the spindle to the cortical cues, providing a complementary explanation of why mouse oocytes undergo nucleus centration.

IVM of human oocytes represents an effective alternative to standard in vitro fertilization (IVF) protocols (in which matured metaphase II oocytes are recovered) for several reasons including the avoidance of ovarian hyperstimulation syndrome and gonadotropin consumption (*63*, *64*). However, the clinical miscarriage is significantly greater after IVM compared to standard IVF (*65*). Therefore, current IVM protocols have substantial room for improvement, as the cumulative live birth rate after a complete cycle remains less than 40% (*64*). Gametes from human females have high rates of aneuploidy, the leading genetic cause of miscarriage and congenital defects (*2*, *3*). To date, there are no definitive morphological markers of predictive oocyte aneuploidy. In addition, human oocytes with a peripherally located nucleus are associated with poor maturation rates compared to those with a centrally located nucleus (*10*). Therefore, it is tempting to speculate that central nucleus positioning is a strategy to ensure initial spindle positioning at the oocyte center, thereby avoiding the development of aneuploid gametes. Understanding the link between peripheral spindle positioning and the incidence of aneuploidy may allow us to better screen for the oocytes predisposed to proper chromosome segregation.

MATERIALS AND METHODS

Ethics

All laboratory animals were managed, and experiments were conducted in compliance with the University of Missouri (Animal Care Quality Assurance reference number 9695).

Mouse strains

Unless otherwise specified, female CF-1 wild-type mice were used. *Cep192-eGfp* reporter mice were generated (*23*) by integrating a construct harboring the enhanced green fluorescent protein (EGFP) reporter gene into CF-1 mouse genome via CRISPR-Cas9–mediated homology-directed repair. The EGFP reporter was fused at the C terminus of the endogenous mouse Cep192. Homozygous breeding pairs of *Cep192-eGfp* reporter mice were used to maintain the colony.

Oocyte collection, microinjection, and IVM

Full-grown GV oocytes were collected from CF-1 female mice aged 6 to 8 weeks. Oocyte collection and culture were carried out as previously described (*23*, *34*). Cumulus oocyte complexes were collected and cultured in bicarbonate-free minimal essential medium (MEM) supplemented with polyvinylpyrrolidone (PVP; 3 mg/ml) and 25 mM Hepes (pH 7.3) under mineral oil (MilliporeSigma, St. Louis, MO, USA, no. P2307, no. H3784, and no. M8410). Oocytes were manually denuded and sorted into three groups: central GV, intermediate GV, and peripheral GV oocytes. Careful rolling of the oocyte, as previously described, ensured correct classification (*5*). Denuded GV oocytes were microinjected with ~5 pl of the indicated complementary RNA (cRNA) using Eppendorf FemtoJet 4i. The medium for oocyte microinjection was MEM supplemented with PVP (3 mg/ml) and 25 mM Hepes (pH 7.3) under mineral oil. Oocytes were then transferred to Chatot, Ziomek, and Bavister (CZB) maturation medium supplemented with 1 μM glutamine (MilliporeSigma, no. G8549) under mineral oil and matured at 37°C with humidified 5% CO_2 in an incubator to prometaphase I, metaphase I, or metaphase II stages. The oocytes that do not undergo NEBD (within 2 hours after culture) were excluded from further experiments.

Nocodazole (Sigma-Aldrich, no. M1404), monastrol (Sigma-Aldrich, no. M8515), ML141 (Sigma-Aldrich, no. SML0407), ZM447439 (Tocris, no. 2458), and CK-666 (Sigma-Aldrich, no. 182515) were dissolved in dimethyl sulfoxide (DMSO) and added to CZB culture medium at a final concentration of 400 nM, 100 μM, 500 nM, 10 μM, and 50 μM, respectively. SiR-tubulin and SiR-DNA were added to the maturation medium (at a final concentration of 100 nM) during live imaging to label MTs and DNA, respectively.

Parthenogenetic activation

Central and peripheral GV oocytes were in vitro matured for 14 hours (metaphase II). Metaphase II oocytes were parthenogenetically activated by culturing the oocytes for 3 hours with 10 mM strontium chloride (Sigma-Aldrich, no. 255521) and cytochalasin D (5 μg/ml; Sigma-Aldrich, no. C2743) in $Ca2^{+}$/$Mg2^{+}$-free CZB medium. The oocytes were then washed and transferred to kalium simplex optimized medium (KSOM) supplemented with cytochalasin D (5 μg/ml) for an additional 3 hours. The oocytes were then washed and cultured in KSOM for 48 hours before assessing embryo cleavage rates.

Oocyte centrifugation

After collection, full-grown GV oocytes were sorted on the basis of nucleus positioning. Central GV oocytes were moved to a single 1.5-ml tube containing MEM supplemented with PVP (3 mg/ml) and 25 mM Hepes (pH 7.3). Oocytes were centrifuged at 1000 rotations per minute for 1 hour at 37°C. After centrifugation, the media contained in the 1.5-ml tube were mixed to dislodge any oocytes stuck to the plastic edge and moved to a flat cell culture plate. Oocytes were sorted on the basis of nucleus positioning; the oocytes were rolled across the plate to ensure correct classification of nucleus positioning. Oocytes were then allowed to mature in vitro according to each experimental design.

In vitro cRNA synthesis

The plasmid was linearized using an appropriate restriction enzyme (New England Biolabs). After linearization, the digests were purified using QIAquick PCR Purification (QIAGEN). Synthesis of cRNAs was performed using T7 polymerase (mMESSAGE mMACHINE, Ambion) according to the manufacturer's instructions. The cRNA was purified using an RNeasy kit (QIAGEN). cRNAs used for microinjection were 3xFLAG-Vash2 (mouse VASH2 with three tandem FLAG tag at the N terminus) at 500 ng/μl, SVBP-hemagglutinin (mouse SVBP with a HA tag at the C terminus) at 300 ng/μl, *Cdc42 T17N* (dominant-negative CDC42 mutant) at 800 ng/μl, PAK-YFP (PAK-PBD-YFP, RAC biosensor) at 100 ng/μl, *Cdc42 Q61L ΔCAAX* (constitutively active CDC42 mutant) at 1000 ng/μl, and *Rac T17N* (dominant-negative RAC mutant) at 2000 ng/μl.

Immunocytochemistry and image analysis

After maturation, oocytes were fixed in a freshly prepared solution of 3.7% paraformaldehyde (MilliporeSigma, no. P6148) dissolved in phosphate-buffered saline (PBS). Oocytes were incubated in permeabilization solution (0.1% Triton X-100 in PBS) for 20 min and blocking solution (0.3% bovine serum albumin and 0.01% Tween 20 in PBS) for 20 min before staining. Oocytes were incubated at room temperature for 1 hour with the primary antibody (N-WASP antibody was incubated overnight at 4°C) before undergoing three consecutive washes in blocking solution for 9 min each. Oocytes were then incubated at room temperature for 1 hour in the secondary antibody solution. Texas Red-X Phalloidin (1:50; Thermo Fisher Scientific, no. T7471) was added to the secondary antibody solution to label F-actin. Following another three consecutive washes in blocking solution at 9 min each, oocytes were mounted on glass slides using VECTASHIELD containing 4′,6-diamidino-2-phenylindole (DAPI; Vector Laboratories, Burlingame, CA, USA) to stain the DNA. Fluorescence was observed using a 40× oil objective using a Leica TCS SP8 confocal microscope or a Leica DMI8 fluorescence microscope, and oocytes were imaged using 3-μm *Z*-intervals. Oocytes were analyzed using National Institute of Health (NIH) ImageJ software (NIH, Bethesda, MD, USA). When applicable, image acquisition and analysis were performed in a blinded manner.

To quantify cortical, perinuclear, and cytoplasmic F-actin intensity, the laser power was adjusted to the level at which cytoplasmic F-actin is detected. Therefore, a minimal change in cortical actin cap is not included in cortical F-actin quantification. To quantify cortical and perinuclear F-actin intensity, multiple regions of interest (ROIs) were measured across the cortical and perinuclear boundaries (four ROIs spanning the corresponding boundaries) and averaged to denote the final intensity measurement for each oocyte. Cytoplasmic F-actin intensities of multiple ROIs (four ROIs spanning the cytoplasm but not overlapping with the nucleus/chromosomes) were averaged to denote the final intensity measurement for each oocyte. To quantify α-tubulin and Tyr α-tubulin, a square ROI surrounding the spindle was measured. ROI areas were fixed among all groups.

The following primary and secondary antibodies were used in immunofluorescence: conjugated α-tubulin–Alexa Fluor 488 (1:75; Life Technologies, no. 322 588), CREST autoimmune serum (1:25; Antibodies Incorporated, no. 15-234), tyrosinated α-tubulin (1:500; Bio-Rad, no. MCA77G), anti–β-tubulin (9F3) monoclonal conjugated to Alexa Fluor 488 (1:50; Cell Signaling Technology, no. 3623), N-WASP (1:100 Cell Signaling Technology, no. 30D10), anti-human Alexa Fluor 647 (1:200; Cell Signaling Technology, no. A21445), anti-mouse Alexa Fluor 488 (1:200; Cell Signaling Technology, no. A32723), anti-mouse Alexa Fluor 568 (1:200; Cell Signaling Technology, no. A10037), anti-rabbit Alexa Fluor 488 (1:200; Cell Signaling Technology, no. A21206), anti-rabbit Alexa Fluor 568 (1:200; Cell Signaling Technology, no. A10042), and anti-rat Alexa Fluor 568 (1:200; Cell Signaling Technology, no. A11077).

In situ chromosome counting

Oocytes matured in vitro for 14 hours in CZB medium supplemented with L-glutamine under mineral oil were transferred to CZB containing 100 μM monastrol (MilliporeSigma, no. M8515) and incubated an extra 2 hours; monastrol is an Eg5-kinesin inhibitor, which induces monopolar spindle formation and thus results in a rosette of chromosome distribution (*33*, *34*). After treatment with monastrol, oocytes at metaphase II stage were fixed in a freshly prepared solution of 2.5% paraformaldehyde (MilliporeSigma, no. P6148) and stained with CREST autoimmune serum (Antibodies Incorporated, no. 15-234; 1:25) to label the kinetochores. DAPI was used to label the DNA. Fluorescence was observed using a 40× oil objective using a Leica DMI8 microscope, and oocytes

were imaged using 0.5-μm *Z*-intervals to observe all kinetochores. Oocytes were analyzed individually and were scored either as euploid (containing 40 kinetochores) or as aneuploid (containing greater or less than 40 kinetochores).

Assessment of K-MT attachment

Cells were matured in vitro for 7 hours in CZB medium supplemented with L-glutamine under mineral oil. The oocytes were placed on ice for 6 min in a 96-well dish containing chilled MEM. Exposing the oocytes to cold shock depolymerizes unattached MTs; however, when MTs have established end-on attachment to a kinetochore, it becomes relatively stable. Oocytes were fixed using a freshly prepared 2.5% paraformaldehyde solution and immunostained with anti-human CREST (to label kinetochores) and α-tubulin (to label MTs) antibodies. DAPI was used to label DNA. Cells were imaged using a Leica TCS SP8 confocal microscope and a 63× oil objective, taking images at 0.5-μm *Z*-intervals. Imaging all oocytes at the same laser power is not required for examining K-MT attachments. Kinetochores were scored as normal (attached to bioriented chromosomes), unattached, or abnormally attached (syntelic, kinetochores of both homologous chromosomes attached to one side of the spindle, or merotelic, a kinetochore maintaining attachment to both sides of the spindle), as previously described (*34*). Oocytes were analyzed using NIH ImageJ Software.

Time-lapse microscopy

Full-grown oocytes were imaged using a 40× oil objective on a Leica TCS SP8 confocal microscope or a Leica DMI8 microscope within a microenvironmental chamber maintaining an atmosphere of 5% CO_2 and a temperature of 37°C in humidified air. Imaging acquisition began as indicated in each experiment. Images were captured at 5- or 7-μm *Z*-intervals to ensure the capture of the oocyte nucleus during its movement. Representative images from the Z-stacks were selected for figurative illustration. Image sequences were analyzed using NIH ImageJ Software.

Statistical analysis

Tests used to evaluate the statistical significance of the findings reported include one-way analysis of variance (ANOVA) and Student's *t* test using GraphPad Prism. The Tukey post hoc test was used to determine statistical significance between groups. Student's *t* test was performed for normally distributed numerical data following the D'Agostino-Pearson omnibus normality test. The number of each biological replicate is specified in the figure legends. When applicable, image acquisition and analysis were performed in a blinded fashion. *P* values of <0.05 were considered significant. The absence of asterisks between groups in each graph indicates nonsignificance. All data are displayed as means ± SEM.

Supplementary Materials

This PDF file includes:
Figs. S1 to S8
Legends for movies S1 to S3

Other Supplementary Material for this manuscript includes the following:
Movies S1 to S3

View/request a protocol for this paper from *Bio-protocol*.

REFERENCES AND NOTES

1. H. Sun, T. T. Gong, Y. T. Jiang, S. Zhang, Y. H. Zhao, Q. J. Wu, Global, regional, and national prevalence and disability-adjusted life-years for infertility in 195 countries and territories, 1990-2017: Results from a global burden of disease study, 2017. *Aging (Albany NY)* **11**, 10952–10991 (2019).
2. T. Hassold, H. Hall, P. Hunt, The origin of human aneuploidy: Where we have been, where we are going. *Hum. Mol. Genet.* **16 Spec No. 2**, R203–R208 (2007).
3. H. E. Hall, U. Surti, L. Hoffner, S. Shirley, E. Feingold, T. Hassold, The origin of trisomy 22: Evidence for acrocentric chromosome-specific patterns of nondisjunction. *Am. J. Med. Genet. A* **143A**, 2249–2255 (2007).
4. S. Gilbert, *Developmental Biology* (Sinauer Associates, Inc., ed. 6, 2000).
5. S. Brunet, B. Maro, Germinal vesicle position and meiotic maturation in mouse oocyte. *Reproduction* **133**, 1069–1072 (2007).
6. P. Hyttel, W. Farstad, M. Mondain-Monval, K. Bakke Lajord, A. J. Smith, Structural aspects of oocyte maturation in the blue fox (*Alopex lagopus*). *Anat. Embryol. (Berl)* **181**, 325–331 (1990).
7. R. Wlodarczyk, D. Bukowska, M. Jackowska, S. Mucha, J. M. Jaskowski, In vitro maturation and degeneration of domestic cat oocytes collected from ovaries stored at various temperatures. *Vet. Med.* **54**, 491–497 (2009).
8. M. Duque Rodriguez, C. O. Cittadini, G. M. Teplitz, A. de Stefano, D. M. Lombardo, D. F. Salamone, Canine IVM with SOF medium, insulin-transferrin-selenium, and low O_2 tension improves oocyte meiotic competence and decreases reactive oxygen species levels. *Front. Cell Dev. Biol.* **9**, 694889 (2021).
9. D. F. Albertini, Cytoplasmic reorganization during the resumption of meiosis in cultured preovulatory rat oocytes. *Dev. Biol.* **120**, 121–131 (1987).
10. M. Levi, Y. Ghetler, A. Shulman, R. Shalgi, Morphological and molecular markers are correlated with maturation-competence of human oocytes. *Hum. Reprod.* **28**, 2482–2489 (2013).
11. J. Lee, T. Miyano, R. M. Moor, Spindle formation and dynamics of gamma-tubulin and nuclear mitotic apparatus protein distribution during meiosis in pig and mouse oocytes. *Biol. Reprod.* **62**, 1184–1192 (2000).
12. T. Fair, S. C. Hulshof, P. Hyttel, T. Greve, M. Boland, Oocyte ultrastructure in bovine primordial to early tertiary follicles. *Anat. Embryol. (Berl)* **195**, 327–336 (1997).
13. D. F. Albertini, S. L. Barrett, The developmental origins of mammalian oocyte polarity. *Semin. Cell Dev. Biol.* **15**, 599–606 (2004).
14. M. Almonacid, W. W. Ahmed, M. Bussonnier, P. Mailly, T. Betz, R. Voituriez, N. S. Gov, M. H. Verlhac, Active diffusion positions the nucleus in mouse oocytes. *Nat. Cell Biol.* **17**, 470–479 (2015).
15. M. Almonacid, M. E. Terret, M. H. Verlhac, Control of nucleus positioning in mouse oocytes. *Semin. Cell Dev. Biol.* **82**, 34–40 (2018).
16. A. Colin, G. Letort, N. Razin, M. Almonacid, W. Ahmed, T. Betz, M. E. Terret, N. S. Gov, R. Voituriez, Z. Gueroui, M. H. Verlhac, Active diffusion in oocytes nonspecifically centers large objects during prophase I and meiosis I. *J. Cell Biol.* **219**, e201908195 (2020).
17. M. Almonacid, A. A. Jord, S. El-Hayek, A. Othmani, F. Coulpier, S. Lemoine, K. Miyamoto, R. Grosse, C. Klein, T. Piolot, P. Mailly, R. Voituriez, A. Genovesio, M.-H. Verlhac, Active fluctuations of the nuclear envelope shape the transcriptional dynamics in oocytes. *Dev. Cell* **51**, 145–157.e10 (2019).
18. A. A. Jord, G. Letort, S. Chanet, F.-C. Tsai, C. Antoniewski, A. Eichmuller, C. D. Silva, J.-R. Huynh, N. S. Gov, R. Voituriez, M.-É. Terret, M.-H. Verlhac, Cytoplasmic forces functionally reorganize nuclear condensates in oocytes. *Nat. Commun.* **13**, 5070 (2022).
19. M. Schuh, J. Ellenberg, Self-organization of MTOCs replaces centrosome function during acentrosomal spindle assembly in live mouse oocytes. *Cell* **130**, 484–498 (2007).
20. D. Clift, M. Schuh, A three-step MTOC fragmentation mechanism facilitates bipolar spindle assembly in mouse oocytes. *Nat. Commun.* **6**, 7217 (2015).
21. A. Z. Balboula, A. L. Nguyen, A. S. Gentilello, S. M. Quartuccio, D. Drutovic, P. Solc, K. Schindler, Haspin kinase regulates microtubule-organizing center clustering and stability through Aurora kinase C in mouse oocytes. *J. Cell Sci.* **129**, 3648–3660 (2016).
22. M. Luksza, I. Queguigner, M. H. Verlhac, S. Brunet, Rebuilding MTOCs upon centriole loss during mouse oogenesis. *Dev. Biol.* **382**, 48–56 (2013).
23. D. Londono-Vasquez, K. Rodriguez-Lukey, S. K. Behura, A. Z. Balboula, Microtubule organizing centers regulate spindle positioning in mouse oocytes. *Dev. Cell* **57**, 197–211.e3 (2022).
24. E. K. McCarthy, B. Goldstein, Asymmetric spindle positioning. *Curr. Opin. Cell Biol.* **18**, 79–85 (2006).
25. F. J. Longo, D. Y. Chen, Development of cortical polarity in mouse eggs: Involvement of the meiotic apparatus. *Dev. Biol.* **107**, 382–394 (1985).
26. H. Li, F. Guo, B. Rubinstein, R. Li, Actin-driven chromosomal motility leads to symmetry breaking in mammalian meiotic oocytes. *Nat. Cell Biol.* **10**, 1301–1308 (2008).

27. M. H. Verlhac, C. Lefebvre, P. Guillaud, P. Rassinier, B. Maro, Asymmetric division in mouse oocytes: With or without Mos. *Curr. Biol.* **10**, 1303–1306 (2000).
28. M. Schuh, J. Ellenberg, A new model for asymmetric spindle positioning in mouse oocytes. *Curr. Biol.* **18**, 1986–1992 (2008).
29. J. Ma, F. Zeng, R. M. Schultz, H. Tseng, Basonuclin: A novel mammalian maternal-effect gene. *Development* **133**, 2053–2062 (2006).
30. J. J. Eppig, M. J. O'Brien, Development in vitro of mouse oocytes from primordial follicles. *Biol. Reprod.* **54**, 197–207 (1996).
31. A. Inoue, R. Nakajima, M. Nagata, F. Aoki, Contribution of the oocyte nucleus and cytoplasm to the determination of meiotic and developmental competence in mice. *Hum. Reprod.* **23**, 1377–1384 (2008).
32. S. I. Lane, Y. Yun, K. T. Jones, Timing of anaphase-promoting complex activation in mouse oocytes is predicted by microtubule-kinetochore attachment but not by bivalent alignment or tension. *Development* **139**, 1947–1955 (2012).
33. F. E. Duncan, T. Chiang, R. M. Schultz, M. A. Lampson, Evidence that a defective spindle assembly checkpoint is not the primary cause of maternal age-associated aneuploidy in mouse eggs. *Biol. Reprod.* **81**, 768–776 (2009).
34. A. Z. Balboula, K. Schindler, Selective disruption of aurora C kinase reveals distinct functions from aurora B kinase during meiosis in mouse oocytes. *PLOS Genet.* **10**, e1004194 (2014).
35. X. Hou, J. Zhang, L. Li, R. Ma, J. Ge, L. Han, Q. Wang, Rab6a is a novel regulator of meiotic apparatus and maturational progression in mouse oocytes. *Sci. Rep.* **6**, 22209 (2016).
36. I. Bennabi, F. Crozet, E. Nikalayevich, A. Chaigne, G. Letort, M. Manil-Ségalen, C. Campillo, C. Cadart, A. Othmani, R. Attia, A. Genovesio, M. H. Verlhac, M. E. Terret, Artificially decreasing cortical tension generates aneuploidy in mouse oocytes. *Nat. Commun.* **11**, 1649 (2020).
37. A. Z. Balboula, K. Schindler, T. Kotani, M. Kawahara, M. Takahashi, Vitrification-induced activation of lysosomal cathepsin B perturbs spindle assembly checkpoint function in mouse oocytes. *Mol. Hum. Reprod.* **26**, 689–701 (2020).
38. S. I. Lane, H. Y. Chang, P. C. Jennings, K. T. Jones, The Aurora kinase inhibitor ZM447439 accelerates first meiosis in mouse oocytes by overriding the spindle assembly checkpoint. *Reproduction* **140**, 521–530 (2010).
39. T. Akera, L. Chmátal, E. Trimm, K. Yang, C. Aonbangkhen, D. M. Chenoweth, C. Janke, R. M. Schultz, M. A. Lampson, Spindle asymmetry drives non-Mendelian chromosome segregation. *Science* **358**, 668–672 (2017).
40. A. Sanfins, G. Y. Lee, C. E. Plancha, E. W. Overstrom, D. F. Albertini, Distinctions in meiotic spindle structure and assembly during in vitro and in vivo maturation of mouse oocytes. *Biol. Reprod.* **69**, 2059–2067 (2003).
41. A. Ferrières, L. Reyftmann, F. Pellestor, B. Hédon, H. Decaud, S. Hamamah, Oocyte recovery post human follicular fluid centrifugation in modified natural cycle and achieving embryo. *Reprod. Biomed. Online* **18**, 671–673 (2009).
42. J. T. Chung, B. R. Downey, R. F. Casper, R. C. Chian, Effect of centrifugation on early embryonic development and parthenogenetic activation of bovine oocytes matured in vitro. *Reprod. Fertil. Dev.* **13**, 383–388 (2001).
43. K. Hara, Y. Abe, N. Kumada, N. Aono, J. Kobayashi, H. Matsumoto, H. Sasada, E. Sato, Extrusion and removal of lipid from the cytoplasm of porcine oocytes at the germinal vesicle stage: Centrifugation under hypertonic conditions influences vitrification. *Cryobiology* **50**, 216–222 (2005).
44. T. S. Kitajima, M. Ohsugi, J. Ellenberg, Complete kinetochore tracking reveals error-prone homologous chromosome biorientation in mammalian oocytes. *Cell* **146**, 568–581 (2011).
45. G. Halet, J. Carroll, Rac activity is polarized and regulates meiotic spindle stability and anchoring in mammalian oocytes. *Dev. Cell* **12**, 309–317 (2007).
46. B. Dehapiot, V. Carriere, J. Carroll, G. Halet, Polarized Cdc42 activation promotes polar body protrusion and asymmetric division in mouse oocytes. *Dev. Biol.* **377**, 202–212 (2013).
47. H. Yan, J. Zhang, J. Wen, Y. Wang, W. Niu, Z. Teng, T. Zhao, Y. Dai, Y. Zhang, C. Wang, Y. Qin, G. Xia, H. Zhang, CDC42 controls the activation of primordial follicles by regulating PI3K signaling in mouse oocytes. *BMC Biol.* **16**, 73 (2018).
48. Y. Zhang, Q.-C. Wang, J. Liu, B. Xiong, X.-S. Cui, N.-H. Kim, S.-C. Sun, The small GTPase CDC42 regulates actin dynamics during porcine oocyte maturation. *J. Reprod. Dev.* **63**, 505–510 (2017).
49. Z. Surviladze, A. Waller, J. Strouse, C. Bologa, O. Ursu, V. Salas, J. Parkinson, G. Phillips, E. Romero, A. Wandinger-Ness, L. Sklar, C. Schroeder, D. Simpson, J. Nöth, J. Wang, J. Golden, J. Aubé, A Potent and Selective Inhibitor of Cdc42 GTPase, *Probe Reports from the NIH Molecular Libraries Program* (NCBI, 2010).
50. A. Bourdais, B. Dehapiot, G. Halet, MRCK controls myosin II activation in the polarized cortex of mouse oocytes and promotes spindle rotation and male pronucleus centration. bioRxiv, 2022.2009.2025.509421 (2022); https://doi.org/10.1101/2022.09.25.509421.
51. K. Yi, J. R. Unruh, M. Deng, B. D. Slaughter, B. Rubinstein, R. Li, Dynamic maintenance of asymmetric meiotic spindle position through Arp2/3-complex-driven cytoplasmic streaming in mouse oocytes. *Nat. Cell Biol.* **13**, 1252–1258 (2011).
52. J. C. Bulinski, J. E. Richards, G. Piperno, Posttranslational modifications of alpha tubulin: Detyrosination and acetylation differentiate populations of interphase microtubules in cultured cells. *J. Cell Biol.* **106**, 1213–1220 (1988).
53. L. T. Ferreira, B. Orr, G. Rajendraprasad, A. J. Pereira, C. Lemos, J. T. Lima, C. G. Boldú, J. G. Ferreira, M. Barisic, H. Maiato, α-Tubulin detyrosination impairs mitotic error correction by suppressing MCAK centromeric activity. *J. Cell Biol.* **219**, e201910064 (2020).
54. J. Nieuwenhuis, A. Adamopoulos, O. B. Bleijerveld, A. Mazouzi, E. Stickel, P. Celie, M. Altelaar, P. Knipscheer, A. Perrakis, V. A. Blomen, T. R. Brummelkamp, Vasohibins encode tubulin detyrosinating activity. *Science* **358**, 1453–1456 (2017).
55. C. Aillaud, C. Bosc, L. Peris, A. Bosson, P. Heemeryck, J. van Dijk, J. le Friec, B. Boulan, F. Vossier, L. E. Sanman, S. Syed, N. Amara, Y. Couté, L. Lafanechère, E. Denarier, C. Delphin, L. Pelletier, S. Humbert, M. Bogyo, A. Andrieux, K. Rogowski, M. J. Moutin, Vasohibins/SVBP are tubulin carboxypeptidases (TCPs) that regulate neuron differentiation. *Science* **358**, 1448–1453 (2017).
56. B. Mogessie, M. Schuh, Actin protects mammalian eggs against chromosome segregation errors. *Science* **357**, eaal1647 (2017).
57. J. Na, M. Zernicka-Goetz, Asymmetric positioning and organization of the meiotic spindle of mouse oocytes requires CDC42 function. *Curr. Biol.* **16**, 1249–1254 (2006).
58. H. Murofushi, Purification and characterization of tubulin-tyrosine ligase from porcine brain. *J. Biochem.* **87**, 979–984 (1980).
59. K. Ersfeld, J. Wehland, U. Plessmann, H. Dodemont, V. Gerke, K. Weber, Characterization of the tubulin-tyrosine ligase. *J. Cell Biol.* **120**, 725–732 (1993).
60. T. Zhao, O. S. Graham, A. Raposo, D. S. Johnston, Growing microtubules push the oocyte nucleus to polarize the *Drosophila* dorsal-ventral axis. *Science* **336**, 999–1003 (2012).
61. D. G. Albertson, Formation of the first cleavage spindle in nematode embryos. *Dev. Biol.* **101**, 61–72 (1984).
62. S. W. Grill, P. Gonczy, E. H. Stelzer, A. A. Hyman, Polarity controls forces governing asymmetric spindle positioning in the *Caenorhabditis elegans* embryo. *Nature* **409**, 630–633 (2001).
63. Practice Committees of the American Society for Reproductive Medicine, the Society of Reproductive Biologists and Technologists, and the Society for Assisted Reproductive Technology. Electronic address: jgoldstein@asrm.org, In vitro maturation: A committee opinion. *Fertil. Steril.* **115**, 298–304 (2021).
64. V. N. A. Ho, S. C. Braam, T. D. Pham, B. W. Mol, L. N. Vuong, The effectiveness and safety of in vitro maturation of oocytes versus in vitro fertilization in women with a high antral follicle count. *Hum. Reprod.* **34**, 1055–1064 (2019).
65. W. M. Buckett, R. C. Chian, N. L. Dean, C. Sylvestre, H. E. G. Holzer, S. L. Tan, Pregnancy loss in pregnancies conceived after in vitro oocyte maturation, conventional in vitro fertilization, and intracytoplasmic sperm injection. *Fertil. Steril.* **90**, 546–550 (2008).

Acknowledgments: We thank all members of the Balboula laboratory at the University of Missouri, Columbia for dedicated help and encouragement. We thank R. Rivera and H. Schatten for critical reading of the manuscript and valuable discussion; Y. Agca, P. Dhakal, T. Spencer, and the Animal Modeling Core and the Molecular Cytology Core for valuable discussion and equipment usage; and G. Halet for providing CDC42, RAC, and PAK-PBD-YFP constructs. Figure 5 was created with BioRender.com. **Funding:** This research was supported by laboratory start-up funding from the University of Missouri and the NIH (R35 GM142537) to A.Z.B. and the Division of Intramural Research at the National Institutes of Health/National Heart, Lung, and Blood Institute (1ZIAHL006249-01) to T.A. **Author contributions:** A.Z.B. conceived the project. J.N.K., A.H., T.A., and A.Z.B. designed and analyzed the experiments. J.N.K., A.H., T.A., and A.Z.B. performed the experiments. J.N.K. and A.Z.B. wrote the manuscript. All authors read/edited the manuscript. **Competing interests:** The authors declare that they have no competing interests. **Data and materials availability:** All data needed to evaluate the conclusions in the paper are present in the paper and/or the Supplementary Materials.

Submitted 30 June 2022
Accepted 19 January 2023
Published 17 February 2023
10.1126/sciadv.add7397